



Fabrication and enhanced electrocatalytic activity of 3D highly ordered macroporous PbO₂ electrode for recalcitrant pollutant incineration



Shouning Chai ^{a,c}, Guohua Zhao ^{a,b,*}, Yujing Wang ^a, Ya-nan Zhang ^{a,b}, Yanbin Wang ^a, Yefei Jin ^a, Xiaofeng Huang ^a

^a Department of Chemistry, Tongji University, Shanghai 200092, China

^b Key Laboratory of Yangtze River Water Environment, Ministry of Education, Shanghai 200092, China

^c Department of Chemistry, College of Science, Xi'an University of Architecture and Technology, Xi'an, Shaanxi 710055, China

ARTICLE INFO

Article history:

Received 23 April 2013

Received in revised form 26 July 2013

Accepted 31 August 2013

Available online 9 September 2013

Keywords:

Macroporous anode

Electrocatalysis

Photonic crystal

Metalaxyl

Mineralization

ABSTRACT

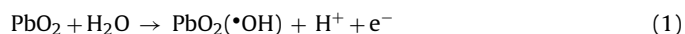
By virtue of the self-assembled colloidal crystal template with face-centered cubic structure, a novel three-dimensional highly ordered macroporous PbO₂ (3DOM-PbO₂) electrode was fabricated by electrochemical deposition method. In the 3DOM-PbO₂ film, every spherical cavity was interconnected to three adjacent spherical cavities on the upper and lower layer, respectively, and the pore size was about 500 nm. Compared to the traditional flat microcrystalline PbO₂ (Flat-PbO₂), the nanocrystalline 3DOM-PbO₂ with β -PbO₂ crystal phase possessed larger specific surface area ($46 \text{ m}^2 \text{ g}^{-1}$), higher oxygen evolution potential (1.92 V), smaller electron transfer resistance (35.5 Ω), and more abundant crystal defect sites, resulting in better electrocatalytic performance. The electrochemical mineralization of refractory metalaxyl with 3DOM-PbO₂ anode demonstrated that, the electrocatalytic reaction followed pseudo-first-order kinetics and the value of apparent rate constant (k_{app}) is 0.017 min^{-1} , about 2.4 times that with Flat-PbO₂, and total organic carbon (TOC) and chemical oxygen demand (COD) removals are all approximately 95% after 300 min. The mineralization current efficiency with the 3DOM-PbO₂ was much higher than that with the Flat-PbO₂, and corresponding electrical energy consumption was lower. Moreover, the intermediates were identified by high-performance liquid chromatography (HPLC) and Gas chromatography–Mass spectrometer (GC–MS), and possible electrocatalytic oxidation mechanism of metalaxyl on the 3DOM-PbO₂ electrode was also discussed in detail.

© 2013 Elsevier B.V. All rights reserved.

1. Introduction

Electrochemical oxidation, characterizing strong oxidation performance, easily manipulating, and environmental compatibility, is an effective approach for decontaminating biologically toxic or persistent substances such as pesticides, pharmaceuticals, organic synthetic dyes, petroleum constituents, personal care products, and a great deal of industrial pollutants [1–7]. It is well known that the degradation efficiency and mineralization degree is largely dependent on the properties of the selected electrode [8–10]. Up to date, various types of electrodes including Pt, graphite, boron doped diamond (BDD), IrO₂, RuO₂, SnO₂, and PbO₂ have been widely investigated [4,11–16]. Among of them, PbO₂ with tetragonal, rutile structure (β -PbO₂, space group $P4/mnm$, D_{4h}^{14}) has been regarded as the optimum anodic materials in applications for electrolysis,

electrosynthesis, and more recently for the wastewater purification due to superior integrated performances including good conductivity, inexpensive and easy to prepare, and chemical inertness [17–21]. According to the comprehensive model proposed by Comninellis et al., a generalized scheme of electrochemical oxidation of organic pollutants on the non-active PbO₂ electrode could be represented as follows [22,23],



The first step involving oxygen transfer reaction is the decomposition of H₂O molecules to generate hydroxyl radicals ($\cdot\text{OH}$). In the following step, the $\cdot\text{OH}$ with high oxidation capability may oxidize pollutants nonselectively, resulting in complete mineralization to CO₂ and H₂O. However, with regard to PbO₂ electrode, there are also several deficiencies that expected to further improve. For example, its catalytic activity is inferior to that of noble metal and SnO₂ electrodes [6,24–27], and its oxygen evolution potential (OEP) is much lower than that of BDD [5,11]. To overcome these

* Corresponding author at: Department of Chemistry, Tongji University, Shanghai 200092, China. Tel.: +86 21 65988570 8244; fax: +86 21 65982287.

E-mail address: g.zhao@tongji.edu.cn (G. Zhao).

drawbacks and promote the practical application, the modification to the traditional PbO_2 electrode is always a research hotspot in the field of electrocatalysis. For example, fluorination or metal ion doping during electrochemical deposition process was considered as one of the ideal means to enhance PbO_2 catalytic performance [28–30]. Some researchers have developed a PbO_2 electrode with high OEP and great catalyst loading capacity by means of fluorine resin assisted fabrication and implanting the PbO_2 crystallite into the vertically ordered TiO_2 nano tubes arrays simultaneously [21]. Moreover, various kinds of PbO_2 composite electrodes were obtained by incorporating different metal oxides particles into PbO_2 matrix such as Co_3O_4 , RuO_2 , La_2O_3 , and ZrO_2 in order to improve the electrochemical activity and stability [31,32]. In brief, it has been widely accepted by most of researchers that improving electrocatalytic performances of traditional PbO_2 electrode mainly by means of controlling composition and crystal form [33,34]. Besides, we believe firmly that it is very important to increase specific surface area of electrocatalyst for a heterogeneous catalysis. However, most of traditional PbO_2 electrodes displaying flat microcrystalline surface morphology, resulting in small effective activity areas and spacial underutilization of active matrix generally. Compared to flat electrode, the nanostructured and porous electrode can provide high surface area, more abundant active sites, and short diffusion paths for ion transport and electron conduction [35]. Nevertheless, we found that it is difficult to obtain the nano-sized porous PbO_2 with excellent crystallinity through classical electro-deposition method without supplementary means due to its particular crystalline structure referring to previous studies. So far, the fabrication and application of porous-structured PbO_2 electrode for pollutants decomposition is rarely reported. We assume that the ordered porous PbO_2 should be obtained facilely if take advantage of hard template assisted electrodeposition approach. Recently developed colloidal crystal-templated synthesis techniques have enabled the chemical preparation of various kinds of organic and inorganic films with three-dimensional (3D) ordered arrays of regular, interconnected and sub-micron diameter macropores [36], which have found huge potential applications in the fields of material, environment, and energy [37–39]. Likewise, if a similar macroporous PbO_2 electrode was gained, which should be provided numerous individual reaction micro space on the electrode surface and be facilitated the electrons transfer as a result of ordered network for electrochemical oxidation.

Therefore, in the present work, for the sake of obtaining larger specific surface area and good crystallinity, a novel 3D highly ordered macroporous PbO_2 electrode (3DOM- PbO_2) with inverse opal architecture was fabricated by electrochemical deposition based on the self-assembled photonic crystal film [40–43]. The morphology, crystalline structure, and electrochemical performance of as-prepared electrode were characterized. In order to evaluate its electrocatalytic activity and mineralization capability, metalaxyl (*N*-(2,6-dimethylphenyl)-*N*-(methoxyacetyl)-Alanine methyl ester), an important acetanilide fungicide widely used in the control of plant diseases caused by pathogens of the *Oomycota* division [44], was used as an toxic, biorefractory model organic pollutant for electrochemical degradation. The degradation kinetics and intermediates on the 3DOM- PbO_2 and traditional flat- PbO_2 (Flat- PbO_2) were determined and compared, respectively. The possible mechanism of metalaxyl mineralization was proposed.

2. Experimental

2.1. Reagents and materials

Pure titanium sheets (99.9%, 60 mm × 15 mm × 1 mm) were used for the electrode substrate. Monodisperse polystyrene latex spheres (ac. 500 nm, 1 wt% in water) were purchased as a

suspension from Shenzhen Nanomicro Tech. China. SnCl_2 , SbCl_3 , $\text{Pb}(\text{NO}_3)_2$ metalaxyl were analytical grade and methanol was of chromatographic grade, purchased from Sigma-Aldrich Chemical Co., Ltd. Ethanol, HCl, HNO_3 , NaF, and Na_2SO_4 were obtained from Sinopharm (Shanghai, China). All chemicals used in the experiments used as received without further purification. For solution preparation and chromatographic purposes, ultrapure water (Milli-Q water, Millipore) was used.

2.2. Preparation of 3DOM- PbO_2 electrode

Firstly, the Sb doped SnO_2 film as intermediate layer was grown by dipping sol-gel method on the pretreated titanium sheet according to the procedure described in the previous studies [45]. Titanium sheets were first mechanically polished with different abrasive papers and washed in ultrapure water and acetone by ultrasonic washing. Then, they were etched in boiling hydrochloric acid (18%, m/m) at the temperature of 85 °C for 15 min to produce a gray surface with uniform roughness. Sb doped SnO_2/Ti (SnO_2 electrode) was prepared by a sol-gel technique as reported in literatures [46]. The precursor consisted of a molar ratio of Sn/Sb 20:1 using a mixture of ethanol and concentrated hydrochloric as solvents. A small amount of ethoxyl aminopropyl trisiloxane (0.05 wt%) was added to lower the surface tension. The pretreated Ti substrates were dipped into the above mixture at room temperature for 20 s. Then they were dried at 100 °C for 10 min and calcined at 500 °C for 10 min. This procedure was repeated 5 times. Finally the electrodes were annealed at 500 °C for 1 h at the oxygen atmosphere. And the Sb-doped SnO_2/Ti composite electrode was obtained.

Secondly, the polystyrene colloidal crystal film was assembled on Sb-doped SnO_2/Ti substrate (SnO_2/Ti) via solvent evaporation method [47]. In a 25 mL breaker, the SnO_2/Ti was immersed vertically in the polystyrene spheres (PS, average diameter about 500 nm) suspension with a concentration of 0.1 wt% (sonicated for 30 min to disperse before using). The breaker was kept in an oven at 50 °C until the water in the suspension was fully evaporated, assembling a colorized polystyrene opals film on the substrate. And then, SnO_2/Ti assembled PS colloidal crystal served as the anode (working area, 8 cm²), and PbO_2 is deposited onto it in the electrolyte containing 0.50 M $\text{Pb}(\text{NO}_3)_2$, 0.10 M HNO_3 , and 0.01 M NaF under the galvanostatic method of 50 mA cm⁻² at 80 °C for 15 min [21].

Finally, the PS template was removed by immersing in toluene for 2 h, and washed by ethanol and water in turn, obtaining the 3DOM- PbO_2 electrode. The traditional flat microcrystalline PbO_2 electrode (Flat- PbO_2) was prepared refer to the same procedure without PS photonic crystal as template.

2.3. Characterization of the surface structure and electrochemical properties test

The morphology of samples was characterized by a scanning electron microscopy (ESEM, Model Quanta 200 FEG, FEI) with an accelerating voltage of 200 kV. X-ray diffraction (XRD, Model D/max2550VB3+/PC, Rigaku) analysis was performed using a diffractometer with Cu K α radiation, with an accelerating voltage of 40 kV and the electron probe current of 30 mA. The XPS spectra of PbO_2 anodes were determined on a X-ray photoelectron spectrometer (AXIS-ULTRA DLD, Shimadzu, Japan) using monochromatized Al K α radiation (1486.6 eV). The binding energy (BE) measurements were corrected for charging effects with reference to the C 1s peak of the adventitious carbon (284.6 eV). The specific surface area of the PbO_2 samples was estimated by the BET adsorption-desorption isotherms of nitrogen at 77 K using a BET analyzer (TRISTAR 3000 Micromeritics, U.S.A.), and the samples were degassed at 180 °C in vacuum for 6 h. The contact angle (CA) of water on the electrode

Table 1Comparison of some physico-chemical parameters of 3DOM-PbO₂ and Flat-PbO₂.

	Flat-PbO ₂	3DOM-PbO ₂
Crystal size (nm) ^a	16	15
S _{BET} (m ² g ⁻¹)	8	46
Contact angle (°)	75	105
R _s (Ω) ^b	1.4	1.2
R _{ct} (Ω) ^b	85.7	35.5
C _{dl} (μF) ^b	112	380
Γ _o (mol cm ⁻²) ^c	7.6 × 10 ⁻¹⁰	5.9 × 10 ⁻⁹
OEP (V)	1.80	1.92
Service life (h)	80	92

^a Crystal size is calculated by Scherrer's formula according to XRD pattern.

^b R_s: solution resistance; R_{ct}: charge transfer resistance at the electrode/electrolyte interface; C_{dl}: double layer capacitance at the electrode/electrolyte interface, which were calculated via equivalent circuit fitting.

^c Γ_o is the adsorption capacity of metalaxyl detected in the initial degradation sample.

surface was measured by drop shape analysis system DSA100 (Krüss, Germany) in air at room temperature and the average contact angle value was calculated based on measurements at three different positions in each sample. All electrochemical measurements were carried out on CHI 660D electrochemical workstation with a conventional three-electrode cell (Shanghai Chenhua Instrument Co. Ltd., China). The 3DOM-PbO₂ and traditional Flat-PbO₂ electrodes served as the work electrode, respectively, while a saturated calomel electrode (SCE) served as the reference and Pt foil as the counter electrode. Polarization curve experiments were performed to test the oxygen evolution potential, and the electrochemical impedance spectroscopy (EIS) was used to determine the conductivity of catalysts at the open circuit potential, with the frequency range from 1 × 10⁵ to 1 × 10⁻³ Hz and amplitude 5 mV, and the electrolyte was 0.5 mol L⁻¹ H₂SO₄ solution. The tests for accelerated service life are performed as described in our previous work [19]. The electrochemical parameters of R_s, R_{ct}, and C_{dl} were calculated from the simulated equivalent circuit (Table 1).

The adsorption capacity Γ_o was determined by chronocoulometry method. According to the Anson equation: Q(t) = Q_{dl} + nAFΓ_o + 2nFAC₀D^{1/2}t^{1/2}/π^{1/2}, the plots of Q ~ t^{1/2} were studied in the 0.05 mol L⁻¹ Na₂SO₄ as blank solution and 0.05 mol L⁻¹ Na₂SO₄ + 100 mg L⁻¹ metalaxyl solution, respectively. Based on the slope difference of the linear relationship between Q and t^{1/2}, Γ_o of metalaxyl on the two electrodes can be obtained [48].

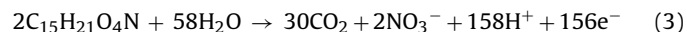
2.4. Degradation experiment and analysis of degraded samples

The electrochemical degradation was carried out in a cylindrical single compartment cell equipped with a magnetic stirrer and a jacketed cooler to maintain a constant temperature (25 ± 2 °C). The 3DOM-PbO₂ and Flat-PbO₂ electrodes worked as the anode, respectively, with working area of 8 cm², and a Ti sheet with the same area was used as the cathode with the electrode gap of 1 cm. A 100 mL sample of 100 mg L⁻¹ metalaxyl in Na₂SO₄ solution was degraded in the cell. The current density was controlled to be constant at 20 mA cm⁻² by a direct current potentiostat. The stirring rate was about 1000 r min⁻¹.

The concentration of the metalaxyl and some carboxylic acid intermediates during the degradation was measured by high-performance liquid chromatography (HPLC, Agilent HP1100). The degraded samples were detected and quantified by AQ-C18 column (4.6 mm × 250 mm, particles size 5 μm), and selected UV detector was at λ = 215 nm. Methanol/water mixtures (60:40 (v/v), adjusted to pH = 4.0 with 0.15 mol L⁻¹ H₃PO₄) and 0.5% (NH₄)₂HPO₄–H₃PO₄ (pH = 2.4) solution were employed as the mobile phase for the metalaxyl and carboxylic acid intermediates detection, respectively, at the same flow rate of 1 mL min⁻¹. The injection volume

was 20 μL. Gas chromatography–Mass spectrometer (GC–MS) analysis was also performed to identify the main intermediate products formed during the metalaxyl degradation process. Degradation samples were pretreated by liquid–liquid extraction with CH₂Cl₂ solvent to extract and concentrate compounds with different polarity and volatility. The extracts were dried on anhydrous sodium sulfate overnight. The finished sample was concentrated under reduced pressure to 1 mL and then analyzed. Spectra were obtained with a gas chromatograph (Agilent 7890A), equipped with DB-5 MS capillary column (30 mm × 320 μm, 0.5 μm film thickness), interfaced directly to the mass spectrometer (5975A inert XL MSD with Triple-Axis Detector) used as a detector. The GC column was operated in a temperature programmed mode with an initial temperature of 50 °C held for 2 min, ramp first to 100 °C with a 6 °C min⁻¹ rate, then to 200 °C with 10 °C min⁻¹ rate and finally ramp to 285 °C with a 20 °C min⁻¹ rate, and held at that temperature for 5 min. Injector temperature was 250 °C with helium served as the carrier gas at the flow rate of 1 mL min⁻¹. Electron impact (EI) mode at 70 eV was used and the mass range scanned was 10–400 m/z. The substance analysis was undertaken with reference to the NIST08 mass spectral library database.

The total organic carbon (TOC) content was measured with a TOC analyzer (TOC-Vcpn, Shimadzu, Japan). According to the previous literatures [4], assuming that metalaxyl (C₁₅H₂₁O₄N) can be completely electrochemically oxidized to CO₂ and H₂O, and the whole reaction process can be expressed as follows:



The mineralization current efficiency (MCE) for each treated sample was calculated from the TOC values according to Eq. (4) [49,50].

$$\text{MCE } (\%) = \frac{\Delta(\text{TOC})_{\text{exp}}}{\Delta(\text{TOC})_{\text{theor}}} \times 100 \quad (4)$$

Δ(TOC)_{exp} and Δ(TOC)_{theor} are the experimental and the theoretical change values in TOC over handling time (mg L⁻¹), respectively. The Δ(TOC)_{theor} could be calculated by Eq. (5),

$$\Delta(\text{TOC})_{\text{theor}} = \frac{[(I \times t)/(n_e \times F)] \times n_c \times M \times 10^3}{V} \quad (5)$$

where I is the applied current (A), t is the electrolysis time (s), n_e is the number of electron consumed in the mineralization of each organic pollutant molecule (78 for metalaxyl), F is the Faraday constant (96,487 C mol⁻¹), n_c is the number of carbon atoms in the organic pollutant molecule (15 for metalaxyl), M is the atomic weight of carbon (12 g mol⁻¹), V is the degradation solution volume (L).

The average electrical energy consumption (EC_{TOC}) in kWh g⁻¹ TOC was defined as the average amount of electrochemical oxidation energy required to remove 1 g TOC [4,27],

$$\text{EC}_{\text{TOC}} = \frac{E_{\text{cell}} \times I \times t}{\Delta(\text{TOC})_{\text{exp}} \times V} \quad (6)$$

where E_{cell} is the potential difference of the cell (V), and the representation of other symbols are same as above-mentioned.

2.5. Determination of •OH

Because of nonselectivity and high reactivity of •OH oxidation, it is difficult to determine directly its concentrations and the indirect methods must be used. Hydroxyl radicals produced by the electrodes are determined with dimethyl sulfoxide (DMSO) trapping as previously reported method [51]. Formaldehyde was generated quantitatively by the reaction between hydroxyl radicals and DMSO, and then reacted with 2,4-dinitrophenylhydrazine (DNPH) to form the corresponding hydrazone (HCHO-DNPH) derivatives

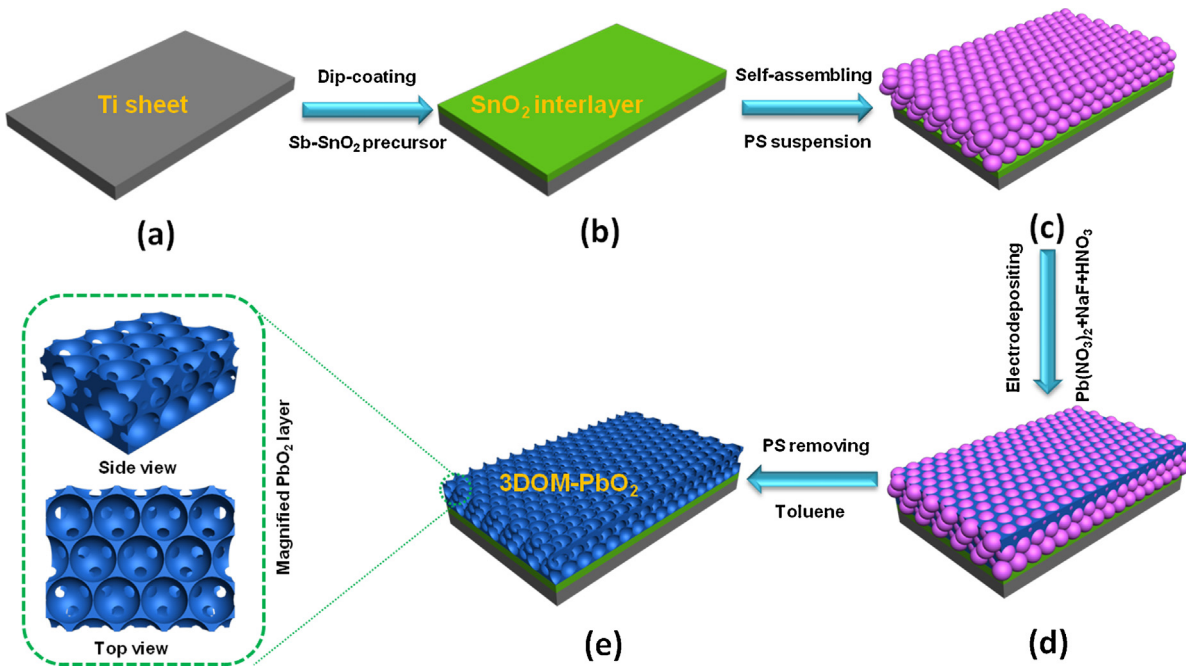


Fig. 1. Schematic illustration for the fabrication of 3DOM-PbO₂ electrode.

and analyzed by HPLC with AQ-C18 column and a selected UV detector at $\lambda = 355$ nm. To perform the isocratic elution at a flow rate of 1.0 mL min^{-1} , a mixture of methanol and water (60:40, v/v) was used as the mobile phase.

3. Results and discussion

3.1. Fabrication and surface characteristics of the 3DOM-PbO₂

The 3DOM-PbO₂ electrode was fabricated via the combination of electrochemical deposition and hard template method based on self-assembled photonic crystal, which was considered as one of promising approaches for constructing various kinds of porous, through-pored films. The protocol is schematically illustrated in Fig. 1. To overcome the drawbacks of exfoliation and poor stability of PbO₂ film directly deposited on titanium plate, the Sb-doped SnO₂ interlayer was thermally deposited onto the pretreated titanium foil firstly, reducing the internal stress and improve the stability. Fig. S1 of Supplementary Materials (SM) shows typical SEM image of Sb-doped SnO₂ coating. Through the dip-coating sol method, countless SnO₂ grain with the particle size of 10–20 nm was uniformly constructed on the Ti substrate, and the microscopic surface of SnO₂ electrode was relatively leveled, which would facilitate PS self-assembling to orderly photonic crystal layer. The SnO₂ layer, which was uniform and compact with good chemical stability and electrochemistry stability, could prevent the formation of TiO₂ during the electrodepositing process by slowing down the diffusion of nascent oxygen toward the interface of the Ti substrate effectively. Moreover, a certain amount of Sb (V) doped in the SnO₂ crystal lattice could provide more electrons in the conduction band. Therefore, the interlayer could reduce the interfacial resistance between the PbO₂ coating and the Ti substrate remarkably. This made the electrodepositing process easier, and therefore smooth PbO₂ films with good adhesion could be formed [52]. The quality of materials formed through template synthesis depends sensitively on the order and properties of the initial template. Face-centered cubic (FCC) colloidal crystal self-assembled on SnO₂/Ti using a vertical deposition method, with suspensions of 500 nm PS. In this case, the PS was organized into a close-packed arrangement

with long-range order both parallel and perpendicular to the substrate (Fig. 1c), as shown in Fig. 2A of SEM image. The structure exhibited 3D ordered because the spheres were mono-dispersed. Then, the photonic crystal film was employed as template to form 3DOM structure. During the electro-deposition, countless lead ions continuously permeated into the voids between the spheres and be oxidized in situ (Fig. 1d), and subsequently formed highly ordered inverse opal structured PbO₂ outer layer after PS template removed completely in toluene solvent (Fig. 1e). 3DOM PbO₂ film was robust and adhered strongly to the SnO₂ interlayer with highly refractive in appearance. To our knowledge, PbO₂ is a polymorphic material with mainly two allotropic forms: orthorhombic α -PbO₂ and tetragonal β -PbO₂ [17]. Advanced electrochemical water treatments preferably adopt β -phase as electrocatalyst material because it has much higher electrocatalytic activity and better electron conductivity than α -PbO₂. It has been reported that the phase composition of PbO₂ may depend on many parameters [53]. Thus, a proper electro-depositing condition including factors of pH range, current density, and temperature should be controlled to obtain the β -phase. Moreover, fluorine ion addition in electrolyte was beneficial to the electrochemical activity and stability of PbO₂ electrode [28,54]. Fig. 2B and C shows typical SEM images of 3DOM-PbO₂ and common Flat-PbO₂ electrodes, respectively. Different from the micron-sized polyhedron, tightly packed and angular crystals of traditional Flat-PbO₂ electrode (Fig. 2C), the micrograph of inverse opal 3DOM-PbO₂ shows that the spherical segment voids left in the PbO₂ film after removal of the PS, which have uniform mouths and arranged in an 3D ordered, hexagonal, close-packed array as expected from the structure of the original template. The individual ordered domains pores are about 500 nm in size, which could be adjustable by the diameter of the PS used. The center-to-center distance measured for the pores is also the same, equals to the PS diameter. It was interesting that every spherical cavity of middle layer is interconnected respectively to three adjacent spherical cavities on the upper and lower layer through three small holes due to the of hexagonal close-packed structure of photonic crystal template, which could be seen from the cross-sectional image of 3DOM-PbO₂ (inset of Fig. 2B). Moreover, it is clear that, with template using, not only the size of polycrystalline grain decreases

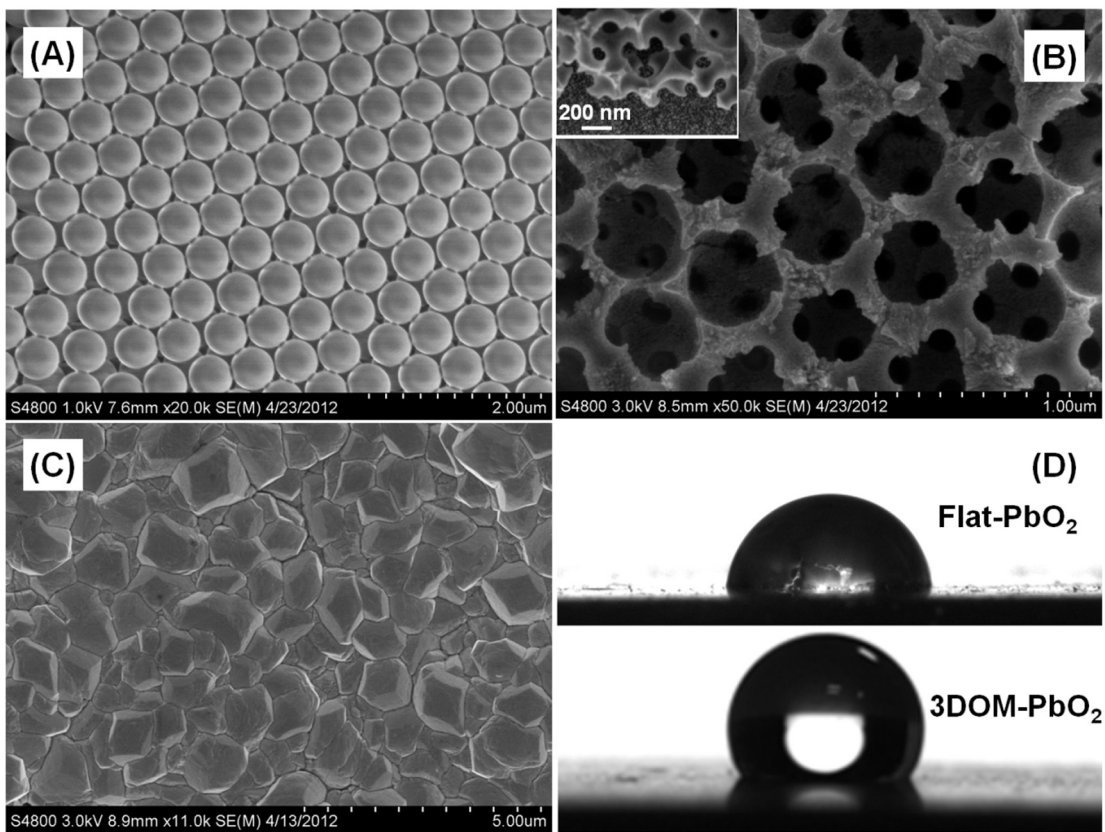


Fig. 2. SEM images of (A) self-assembled PS photonic crystal on the substrate, (B) as-prepared 3DOM-PbO₂, and (C) traditional Flat-PbO₂; (D) photographic images of pure water droplets on the electrodes surface corresponding to Flat-PbO₂ (the upper) and 3DOM-PbO₂ (the lower). Inset: lateral view of 3DOM-PbO₂ film.

from micron-scale to nano-scale, but also the probability of lattice distortion at interfacial regions and the number of crystal boundaries greatly increase [55]. Consequently, abundant formed surface defect sites would be the active centers responsible for the high catalytic activity owing to the exposure of larger numbers of Pb atoms [55]. Compared to the plane structure, the inverse opal structure was beneficial to the improvement of the specific surface area undoubtedly, and the value of 3DOM-PbO₂ is 46 m² g⁻¹, nearly 6 times that of the Flat-PbO₂.

To identify the phase composition of PbO₂ layer, XRD analysis was conducted. Fig. 3A shows the XRD pattern of 3DOM-PbO₂, three strong characteristic diffraction peaks at 2θ value 32.0°, 49.1°, and 62.5° corresponding to (1 0 1), (2 1 1), and (3 0 1) facets appear, which confirms that PbO₂ layer composed of linear crystallographic phase of tetragonal β-PbO₂. Although the polycrystalline grain is diminished with template using, the good crystallinity of β-PbO₂ was also maintained. Furthermore, the doping of F⁻ anions also did not result in visible change of β-PbO₂ crystallographic phase. It could be attributed to the similar ionic radius of F⁻ anions (133 pm) and O²⁻ anions (140 pm) and very low concentration of F⁻ anions in electrolyte [54]. According to previous literatures, the results of XPS spectrum and the secondary ion mass spectrometry (SIMS) analyses had demonstrated traces of oxygen sites were substituted by F⁻ anions in the β-PbO₂ film prepared in the electrolyte containing F⁻ anions [28,56].

When pores are used to increase the surface area for electrochemical oxidation, one should take into account wettability aspects because it is closely related with electrode performance. The wetting of PbO₂ electrodes was studied by measuring the static contact angle of a water drop at equilibrium. Fig. 2E shows an optical image of a 5 μL water drop on the 3DOM-PbO₂ and Flat-PbO₂, and the contact angle is 105° and 75°, respectively. It indicates

that the surface has become more hydrophobic because of the nanostructure consisting of hexagonal array of air-filled pores and fluorine doping [54], which is also one of the possible reasons for the enhancement of the OEP and corrosion resistance of 3DOM-PbO₂. Accordingly, the 3DOM-PbO₂ is more stable than Flat-PbO₂, increasing the service life to about 92 h.

3.2. Efficient electrochemical incineration of metalaxyl

The degradation of metalaxyl with two PbO₂ electrodes was carried out at an initial concentration of 100 mg L⁻¹ to evaluate the electrocatalytic activity and practicality. The time dependence of metalaxyl removal is presented in inset of Fig. 4A. In comparison, the degradation ratios of original pollutant are 70% and 92% at the Flat-PbO₂ and 3DOM-PbO₂, respectively, after 180 min of electrolysis. The corresponding degradation reaction kinetics follows pseudo-first-order kinetics (Fig. 4A), and the apparent rate constant (k_{app}) value at the 3DOM-PbO₂ is 0.017 min⁻¹, which is 2.4 times that on the Flat-PbO₂ of 0.007 min⁻¹. As previously reported, the electrochemical oxidation rate of organic substance is closely related to surface adsorption capacity Γ_0 of the anode, which was calculated by the chronocoulometry with instantaneous single potential step [48]. Γ_0 of metalaxyl on the 3DOM-PbO₂ is 5.9×10^{-9} mol cm⁻², 7.8 times that on the Flat-PbO₂. The result is in accordance with their S_{BET} values, demonstrating that the 3DOM-PbO₂ with larger specific surface area possesses more adsorption active sites to pollutant. On the other hand, numerous defects at the crystal boundaries with high surface energy on the 3DOM-PbO₂ also promote the adsorption strength and capacity of pollutant [55]. Generally speaking, complete mineralization of the recalcitrant organic pollutants is desired for wastewater treatment. Thus it is not sufficient if merely studied the removal

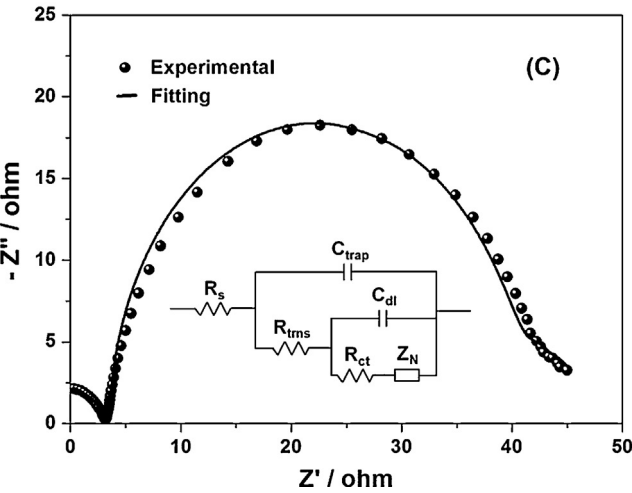
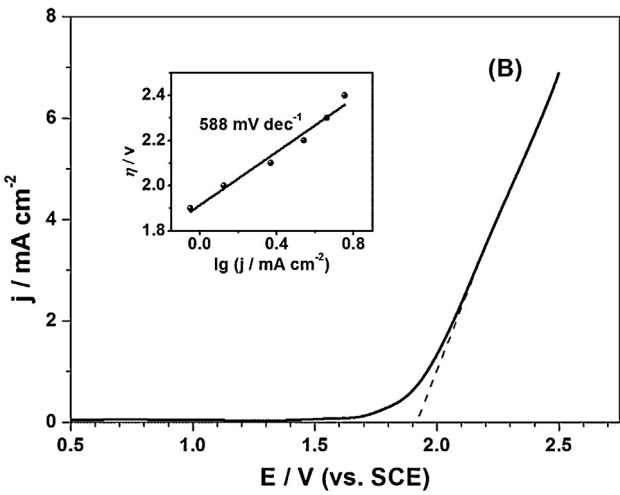
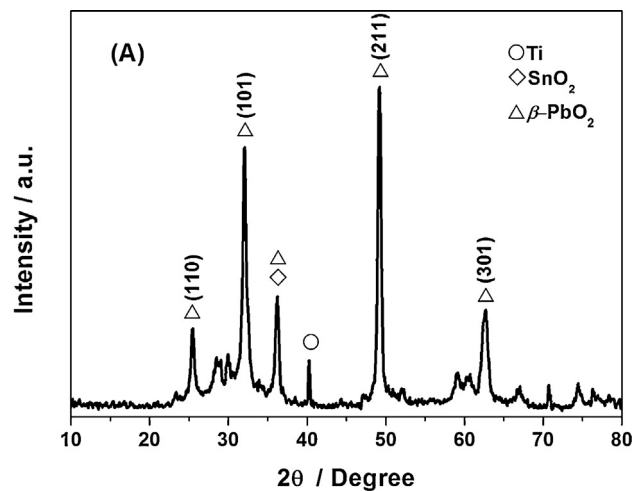


Fig. 3. (A) XRD patterns of as-prepared 3DOM-PbO₂; (B) polarization curve, and (C) Nyquist plot on the 3DOM-PbO₂ anode in 0.5 mol L⁻¹ H₂SO₄ solution. Inset of (B) and (C): corresponding Tafel plot of oxygen evolution reaction and equivalent circuit model, respectively.

ratio of original pollutant. The mineralization of metalaxyl was monitored by measuring TOC. As shown in Fig. 4B, within 300 min, the values of TOC decrease to 19.2 and 3.5 mg L⁻¹ from the initial value of 65.8 mg L⁻¹ at the Flat-PbO₂ and 3DOM-PbO₂ respectively, indicating that metalaxyl was completely mineralized to CO₂ and H₂O at the 3DOM-PbO₂. Obviously, the TOC abatement at the 3DOM-PbO₂ is much higher than that at the Flat-PbO₂, which attributes to high catalytic activity resulted from superficial

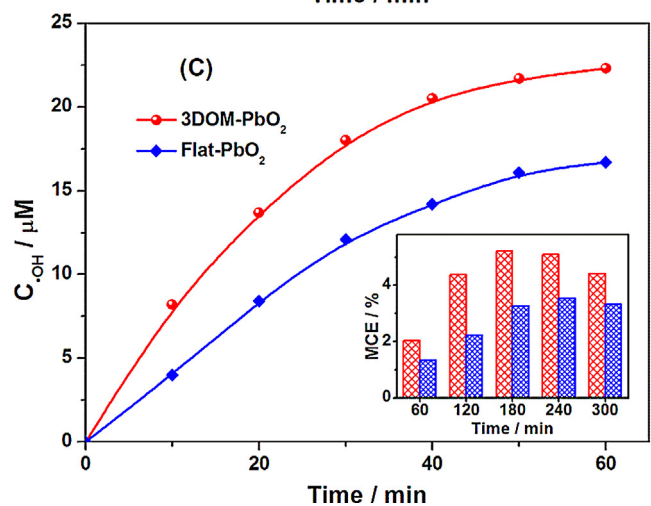
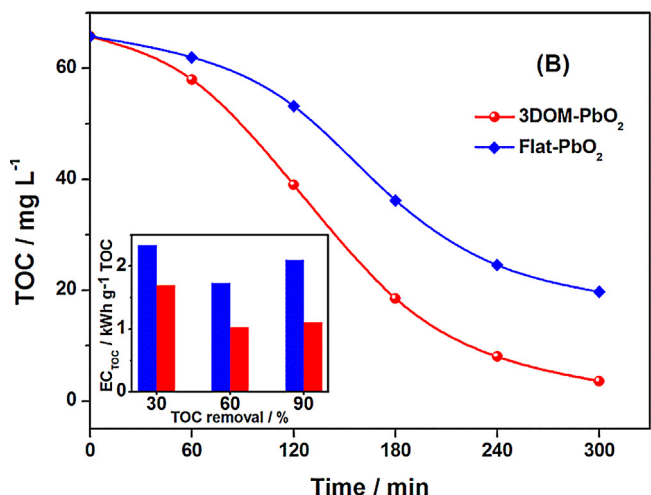
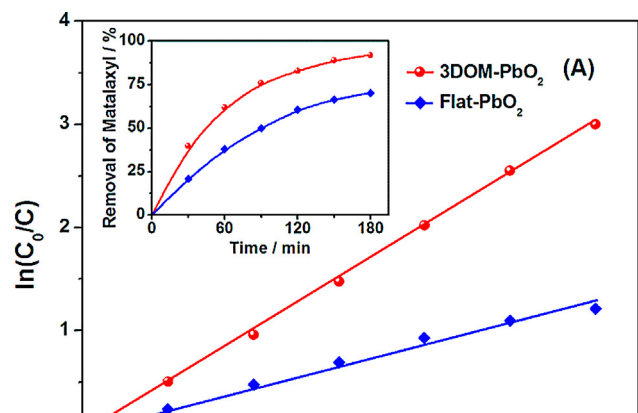


Fig. 4. (A) The kinetics of metalaxyl degradation at the 3DOM-PbO₂ and Flat-PbO₂, (B) TOC removal as a function of the electrocatalytic degradation time, (C) concentration evolution of ·OH as a function of the electrolysis time, inset of (A)–(C): Metalaxyl removal with degradation time, the average energy consumption changes with TOC removal ratio, and the mineralization current efficiency with degradation time, respectively, at the 3DOM-PbO₂ and Flat-PbO₂ electrodes.

defects of the former. The results demonstrate that the ordered macroporous structure with larger effective surface area and more abundant crystal defect sites is in favor of improving electrochemical oxidation capacity for PbO₂ electrode.

Regarding to the advanced oxidation process, the mineralization current efficiency and average energy consumption are two important parameters to evaluate the electrochemical degradation performance of electrode materials. On the basis of the TOC abatement results, the MCE and EC_{TOC} of each degradation stage were determined according to Eqs. (4) and (6), respectively. The evolution of MCE is displayed in inset of Fig. 4C. 3DOM-PbO₂ exhibits a higher MCE than Flat-PbO₂ during the entire electrolysis process, but the same evolution trend of increasing at first and then decreasing is observed. The maximum MCE value of 5.2% is reached at 180 min for the 3DOM-PbO₂, which is about 1.5 times the maximum value for the Flat-PbO₂ at 240 min. It is consistent with that of metalaxyl and TOC removal results. Meanwhile, on the contrary, it is notable that the EC_{TOC} on the 3DOM-PbO₂ is smaller due to the small electrochemical impedance and excellent intrinsic catalytic activity (inset of Fig. 4B). At a TOC removal of 60%, the average EC_{TOC} for the 3DOM-PbO₂ is at the minimum of 1.03 kWh g⁻¹ TOC, only 0.6 times that for the Flat-PbO₂. The possible reason for the maximum MCE and minimum EC_{TOC} appearing in the middle degradation stage is that, in the initial stage, metalaxyl molecules first decomposed to various aromatic intermediates by the electro-generated •OH, so relatively smaller MCE and greater EC_{TOC} were obtained because of low TOC decay rate in terms of the whole degradation process. In the final stage, MCE also decreases and EC_{TOC} increases owing to the generated refractory carboxylic acid by-products such as oxalic acid, acetic acid could not been mineralized readily. The aforementioned results indicated that the rapid electrochemical incineration of metalaxyl could be realized on the 3DOM-PbO₂.

According to the previously works [57], the degradation of metalaxyl may be attributed to direct electrochemical oxidation on the anode surface, indirect electrochemical oxidation mediated by dominating •OH and other subordinate electrogenerated oxidants such as S₂O₈²⁻ (in the presence of SO₄²⁻) and O₃. In our preliminary experiment of cyclic voltammetry, it was found that no evident peak belonging to metalaxyl oxidation was observed on the PbO₂ anode, indicating that it is a kind of non-electroactive substance. Therefore, in terms of 3DOM-PbO₂, it was considered that the degradation of metalaxyl mainly depended on the indirect electrochemical oxidation launching by •OH other than direct oxidation on the anode surface, which effectively avoided the fouling of electrode. To elucidate the role of •OH during the electrochemical oxidation, detection of •OH were performed with two PbO₂ electrodes [51]. As shown in Fig. 4C, the observed concentration of •OH in the 3DOM-PbO₂ cell is much larger than that in the Flat-PbO₂ cell, which means that there is a positive correlation between the total amount •OH and the specific surface area of PbO₂ film. In addition, the chemical oxygen demand (COD) decay was also determined during the degradation (SM Fig. S5). At 300 min, the concentration of COD decreases to 14 mg L⁻¹ from initial 215 mg L⁻¹ at the 3DOM-PbO₂, and the COD removal is up to 93%.

Generally, the electrocatalytic activity and the effective •OH generation capability of an electrode are mostly determined by the material composition itself and crystalline phase. However, in the light of aforementioned results, the difference of catalytic performance between 3DOM-PbO₂ and Flat-PbO₂ is result from the different microstructure and surface characteristics. In order to further study the effect of the microstructure to the electrochemical properties, some electrochemical analyses including the polarization curve (PC) and electrochemical impedance spectroscopy (EIS) were performed. Based on the mechanism of the PbO₂ electrode oxidizing pollutants presented in Eqs. (1) and (2), the first step is the split of water to produce amounts of •OH at anode surface. Some researchers assumed that these •OH could be divided into two kinds, i.e. the adsorbed •OH (including physisorbed or

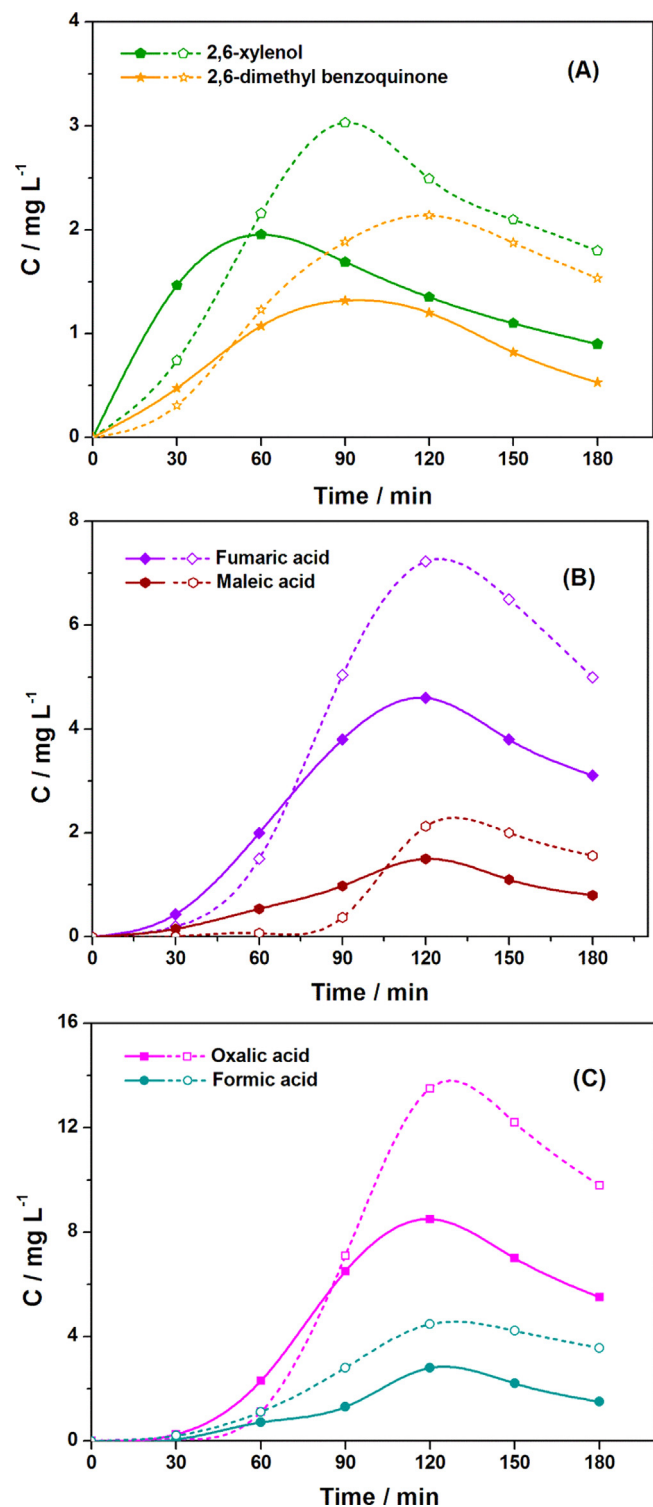


Fig. 5. The concentrations evolution of intermediates as a function of time (A) 2,6-xyleneol and 2,6-dimethyl benzoquinone, (B) fumaric acid and maleic acid, and (C) oxalic acid and formic acid during electrocatalytic degradation of metalaxyl at the 3DOM-PbO₂ (solid line) and Flat-PbO₂ (dash line) electrodes.

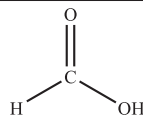
chemisorbed) and the free •OH existing in the vicinity of anode [11]. Then, most of the free •OH and partial of adsorbed •OH can oxidize pollutants to produce CO₂ and H₂O. But most of the rest adsorbed •OH is limited on the electrode surface and consequently is easy to combine with each other to generate oxygen, which would be embodied by the relatively low oxygen potentials on the electrode. As shown in Fig. 3B, the OEP on the 3DOM-PbO₂ is 1.92 V (vs. SCE)

Table 2

Intermediates for the electrochemical degradation of metalexyl by means of GC-MS or HPLC analysis.

Intermediates	Formula	Molecular structure	Retention time (min)	M_w	Main fragment ions (m/z)	Analysis approach
N-(2,6-dimethylphenyl) acetamide	C ₁₀ H ₁₃ ON		13.2	163	163 (M ⁺), 121, 120, 106, 77, 43	GC-MS
2,6-Xylenol	C ₈ H ₁₀ O		12.3	122	122 (M ⁺), 121, 107, 104, 103, 91, 79, 78, 77, 65, 51	GC-MS
2,6-Dimethyl hydroquinone	C ₈ H ₁₀ O ₂		12.5	138	138 (M ⁺), 137, 123, 109, 95, 91, 69	GC-MS
2,6-Dimethyl benzoquinone	C ₈ H ₈ O ₂		7.5	136	136 (M ⁺), 108, 107, 96, 90, 80, 79, 68	GC-MS
2-(Carboxymethylamino)- 3-methylbutanoic acid	C ₇ H ₁₃ O ₄ N		6.8	175	175 (M ⁺), 160, 132, 130	GC-MS
p-Benzoquinone	C ₆ H ₄ O ₂		7.3	108	108 (M ⁺), 82, 80, 54, 53, 26	GC-MS
Maleic acid	C ₄ H ₄ O ₄		11.2	116	–	HPLC
Fumaric acid	C ₄ H ₄ O ₄		8.1	116	–	HPLC
Oxalic acid	C ₂ H ₂ O ₄		2.6	90	–	HPLC
Malonic acid	C ₃ H ₄ O ₄		3.54	104	–	HPLC

Table 2 (Continued)

Intermediates	Formula	Molecular structure	Retention time (min)	M_w	Main fragment ions (m/z)	Analysis approach
Formic acid	CH_2O_2		3.82	46	-	HPLC

with a Tafel slope of 588 mV dec^{-1} , which is higher than that on the Flat-PbO₂ of 1.80 V (SM Fig. S3). According to Pavlov [58] proposed classical mechanism of the oxygen evolution reaction based on the gel-crystal concept for the structure of PbO₂ surface, the doped F[−] anions could be substitute OH[−] sites lying in gel layer and O^{2−} sites lying in crystal layer for a PbO₂ electrode prepared in containing F[−] electrolyte [28,56]. It has been also reported that in the gel layer of PbO₂, F[−] modification not only decreases the coverage of active oxygen species, sequentially to inhibit oxygen evolution [28], but also blocks the diffusion of the free oxygen atoms into the crystal layer [54]. For the 3DOM-PbO₂, the more oxygen vacancies are possibly formed due to the amounts of F[−] in electrolyte adsorbed on the PS template during electro-deposition preparation, consequently the higher OEP is obtained. Besides, the hydrophobicity of 3DOM-PbO₂ surface resulting from the macroporous microstructure maybe the other non-ignorable reason for OEP increase. Thus, the higher OEP on the 3DOM-PbO₂ suggests that the proportion of free •OH dedicating to pollutants oxidation is enhanced in terms of the total amount of •OH generating from H₂O decomposition at the same potential, which is consistent with the results of the effective •OH concentration and metalaxyl removal discussed above. Impedance measurements were further determined to understand the enhanced electrocatalytic ability and obtain more insights into electrochemical properties of the 3DOM-PbO₂. Nyquist plots at the Flat-PbO₂ and 3DOM-PbO₂ are shown in the SM Fig. S4 and Fig. 2C, respectively. The corresponding Bode plots are presented in the SM Figs. S4(B) and S2. At the same time, the equivalent circuit, often used to depict the electrochemical behaviors of electrodes, was employed for fitting the impedance spectra. It is observed that the fitted results are in good agreement with the experimental. As seen in inset of SM Fig. S4(A), the fitted equivalent circuit for the Flat-PbO₂ agrees with Randles model, consisting with the classical circuit for the common flat electrodes. Due to the photonic crystal template using, the obtained 3DOM-PbO₂ contains many superficial defects responsible for its high catalytic activity. These superficial defects such as dangling bonds (or surface radicals) facilitate the charge transfer reaction to provide highly reactive unpaired electrons. On the other hands, they play another role in trapping electrons to form capacitance (C_{trap}) especially near the surface and grain boundaries. Thus, a comprehensive circuit model was simulated for the 3DOM-PbO₂ (inset in Fig. 2C) spectrum. In this case, C_{trap} is coupled in parallel with the electron transport resistance in the PbO₂ layer (R_{trns}) and incorporated with the traditional charge transfer impedance (R_{ct}) (inset in SM Fig. S4(A)). Note that, R_{trns} and C_{trap} are attributed to the resistance and the capacitance of the porous PbO₂ layer itself, respectively. Also, Z_N , C_{dl} , and R_s represent the Nernst diffusion impedance, the double layer capacitance, and the solution resistance, respectively [59]. The fitted R_{ct} value of 3DOM-PbO₂ is 35.5Ω , less than one half of that of Flat-PbO₂ (85.7Ω) in our experiments condition. The results indicate that the ordered porous structure is beneficial to the charge transfer directionally, and the aqueous ions can transport in and out porous cavities quickly and unimpededly. In a word, 3D ordered macroporous structure of 3DOM-PbO₂ film facilitates mass and electron transport, accordingly improves the electrocatalytic ability and reduces the corresponding energy consumption.

3.3. Intermediates formed and mineralization mechanism

Dozens of intermediates formed were identified by GC-MS and/or HPLC analysis during electrochemical treatment of metalaxyl. Their structures and main mass fragmentation data are summarized in Table 2. The detected aromatic intermediates include 2,6-dimethylbenzoquinone, N-(2,6-dimethylphenyl) acetamide, p-benzoquinone, 2-(carboxymethylamino)-3-methylbutanoic acid, 2,6-xlenol, 2,6-dimethylhydroquinone. To figure out the degradation kinetics more in-depth, the evolution of two prime aromatic intermediates (2,6-dimethylhydroquinone, 2,6-xlenol) and four carboxylic acid byproducts in degradation samples were quantitatively determined by HPLC with the aid of standard substances, as depicted in Fig. 5. A typical accumulation–destruction cycle can be seen in all cases, those aromatic intermediates are accumulated in the first stage of because their generation from the cleavage of the parent molecules, whose high initial concentration causes the consumption of most of the •OH that predominating over their destruction, and after reaching a maximum concentration (c_{max}) they are progressively converted into other subprime by-products and/or CO₂ and H₂O [60]. For the whole metalaxyl degradation process, a faster disappearance of byproducts with lower accumulated concentration was achieved at the 3DOM-PbO₂ compared to the Flat-PbO₂. c_{max} of 1.9 and 1.3 mg L^{-1} were attained for 2,6-xlenol and 2,6-dimethylhydroquinone with the 3DOM-PbO₂ treated samples, while corresponding values are 3.1 and 2.2 mg L^{-1} with the Flat-PbO₂, respectively. Meanwhile, it is worth of note that the time (t_{max}) corresponding to the appearance of c_{max} is shorter at the 3DOM-PbO₂ than that at Flat-PbO₂. With regards to cyclic organic pollutants degradation, the formed various short-chain aliphatic carboxylic acids in the later stage are usually harder to oxidize than their parent compounds [13,60]. For example, fumaric, maleic, oxalic, formic acids could be detected gradually about 30 min and the maximum concentrations are reached at 120 min. After 180 min, although above 90% metalaxyl removal is achieved, there are also abundant of them remaining in treated samples due to their lower reactivity with •OH. Their persistent presence may partly explain the MCE decreasing and average EC_{TOC} increasing at the end of treatments (see Fig. 4). These aforementioned findings further demonstrate stronger catalytic activity and larger handling capacity of the 3DOM-PbO₂, accordingly avoids the excessive accumulation of intermediates and their polymerization effectively. On the basis of by-products identified, a plausible scheme including various oxidation pathways leading to the total mineralization of metalaxyl is proposed in Fig. 6. The attack of •OH onto four different reaction sites of metalaxyl is suggested, which yields different primary intermediates according to pathways A–D. Routes A and B involve the formation of 2,6-xlenol and 2,6-dimethyl benzoquinone caused by consecutive hydroxylation of aromatic ring. Route C is initiated by •OH attacking the substituent of branch chain, yielding N-(2,6-dimethylphenyl) acetamide and several short chain carboxylic acids. Route D occurs to cleavage of the benzene ring structure launching by two •OH simultaneously, which leads to the formation of 2-(carboxymethylamino)-3-methylbutanoic acid. Subsequently,

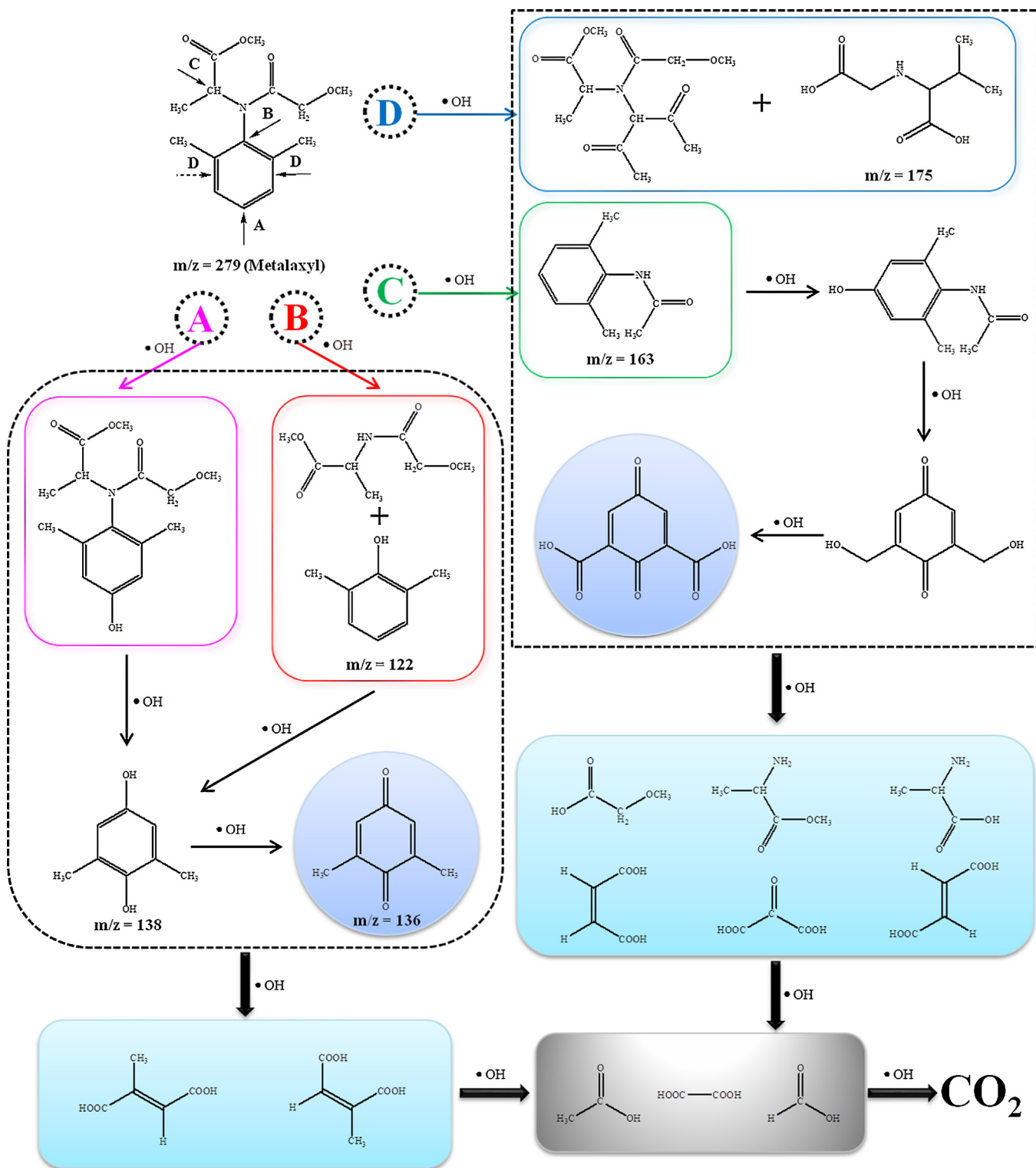


Fig. 6. Possible degradation pathways for the total mineralization of metalaxyl at the 3DOM-PbO₂.

those aromatic intermediates are attacked by •OH continuously to form various quinone derivatives, which is degraded to form a mixture of carboxylic acids like maleic and acetic from the cleavage of its benzenic ring. Therein, the highlighted intermediates are crucial substance in their respective degradation routes. Undoubtedly, the electrochemical oxidation of metalaxyl predominated by •OH is very complicated, the detected by-products is only a limited proportion, so those small molecular acids can also be

produced from the parallel destruction of undetected intermediates formed from other reactions. Ultimately, the mineralization of metalaxyl is completely accomplished until almost all of formed carboxylic acids decompose to CO₂ and H₂O. In a word, it should be noted that metalaxyl can be rapidly decomposed and mineralized by electrochemical oxidation on the 3DOM-PbO₂ under mild conditions, which has many advantages over the traditional Flat-PbO₂, such as relatively better electrocatalytic performance,

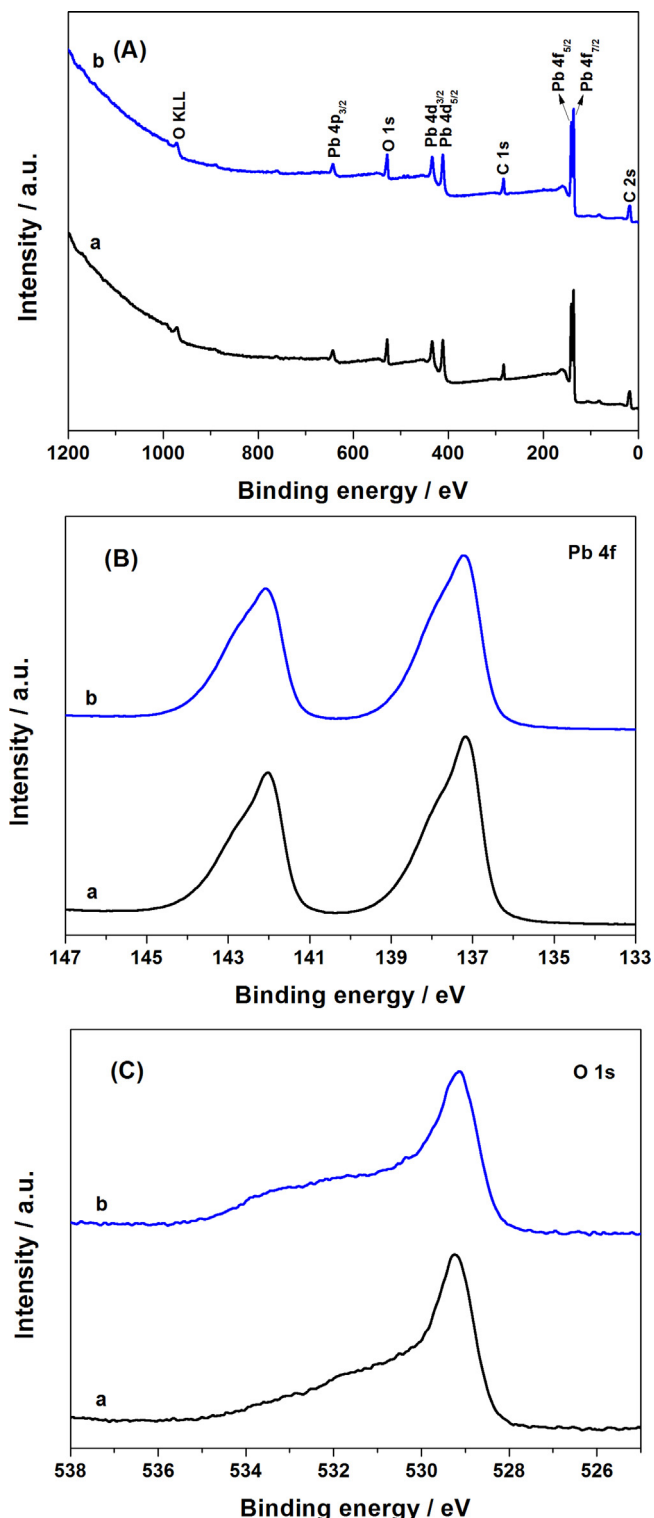


Fig. 7. XPS spectra of as-prepared (a) and used (b) 3DOM-PbO₂ anodes: (A) survey spectrum, (B) Pb 4f, and (C) O 1s.

higher mineralization current efficiency, and lower energy consumption.

3.4. Stability of 3DOM-PbO₂ anode

The stability of PbO₂ anode is always a focus of most concern in previous studies [61,62]. In the present work, the stability of 3DOM-PbO₂ anode is analyzed through comparing some surface

properties of as-prepared and used anodes. The used anode is the 3DOM-PbO₂ employed in metalexyl degradation for 5 h. Before characterization, no pretreatment is conducted for the used anode besides rinsed by deionized water.

SM Fig. S6 presents the morphologies of used 3DOM-PbO₂ anode. Compared with the SEM image of as-prepared one in Fig. 2B, it is found that the electrode surface is covered by a layer of unknown compounds film, which maybe the formed polymers during metalexyl electrochemical oxidation [50,63]. However, the well-defined 3D porous microstructure is maintained after 5 h degradation utilization. It preliminarily indicates that the 3DOM-PbO₂ is robust and stable. Moreover, experimental investigation shows that the used 3DOM-PbO₂ can be well recycled after immersing in acetone for a moment to remove trace polymers readily.

XRD analysis of the used 3DOM-PbO₂ anode is also conducted. As shown in SM Fig. S7, several characteristic diffraction peaks corresponding to (101), (211), and (301) facets of β -PbO₂ have no apparent change, which are still sharp and strong comparing with XRD pattern of as-prepared 3DOM-PbO₂ in Fig. 3A. Meanwhile, no new diffraction peaks appears. The results suggest that crystalline grain on 3DOM-PbO₂ surface remained intact, and no obvious phase transition occurs when a certain potential is applied on it during electrochemical degradation.

XPS with high sensitivity is used to study the surface chemical state of the 3DOM-PbO₂ before and after electrolysis. As shown by the survey spectra in Fig. 7A(a), there are peaks for Pb 4f and O 1s, indicating the existence of lead dioxide. In addition, detailed speciation information is investigated from high resolution XPS scans in the different binding energy regions. The Pb 4f spectra (Fig. 7B) display a doublet characteristic of Pb 4f_{7/2} and Pb 4f_{5/2} centered at 137.3 eV and 142.2 eV, respectively, in agreement with the spectral values for PbO₂ [61,64]. Comparing the survey spectra and Pb 4f spectra of as-prepared and used 3DOM-PbO₂ anodes, it is found that the binding energy, peak shape, and peak intensity are almost identical, which suggests that no new lead speciation is generated. Regarding to the XPS spectrum of O1s in Fig. 7C(a), the main signal at 529.2 eV is assigned to strongly bound (lattice) oxygen, and the shoulder at higher binding energy is assigned to weakly bound oxygen species: adsorbed $-\text{OH}$ and water [62,65]. The spectrum of O1s (Fig. 7C(b)) for the used electrode was apparently different from that of the as-prepared electrode due to the shoulder peak is stronger. The result confirms the existence of abundant adsorbed hydroxyl radicals on the non-active 3DOM-PbO₂ electrode surface as proposed in Eq. (1), which is beneficial to organic pollutants decomposing for an indirect electrochemical oxidation process. These XPS results further demonstrate that the 3DOM-PbO₂ displays excellent stability.

The leaching of lead ion always is a non-ignorable problem to limit PbO₂ anode utilization. So the parameter is significant for evaluating the comprehensive quality of one electrode. A XSERIES 2 inductively coupled plasma mass spectrometer (ICP-MS, Thermo Scientific) is used to investigate the leached lead concentration in the filtered degraded sample. The concentration of lead ions after 5 h electrochemical degradation is detected at $2.8 \times 10^{-5} \text{ g L}^{-1}$ in the electrolyte using Flat-PbO₂, and the value is $8.5 \times 10^{-6} \text{ g L}^{-1}$ using 3DOM-PbO₂. The data indicate that two kinds of PbO₂ anode are very stable during degradation. As proposed by Yuan et al. [66], the SnO₂ interlayer, as a protective layer, could improve the conductivity and inhibit the TiO₂ formation between Ti substrate and PbO₂, which would effectively hinder the lead detaching. One also can find that the leaching lead concentration of 3DOM-PbO₂ is much lower than that of Flat-PbO₂, which maybe attribute to its hydrophobic property and smaller crystalline grain on 3DOM-PbO₂ surface.

4. Conclusions

In this work, we developed a facile route to fabricate inverse opal structural PbO₂ electrode with uniform macroporous cavity and studied its application on degrading persistent metalaxyl via electrochemical process. The obtained 3DOM-PbO₂ exhibited high surface area, strong adsorption capacity, good electrical conductivity and high degradation efficiency. Metalaxyl removal was reached 92% after 3 h and TOC removal is about 95% after 5 h with 3DOM-PbO₂ electrocatalysis, while the value was respectively 70% and 71% using traditional Flat-PbO₂. The degradation of metalaxyl obeyed the pseudo-first-order kinetics. The enhanced degradation and mineralization ability was directly related to improved •OH generation. In addition, several aromatic intermediate products including 2,6-dimethylbenzoquinone, N-(2,6-dimethylphenyl) acetamide, p-benzoquinone, 2,6-xylenol, 2,6-dimethylhydroquinone and 2-(carboxymethylamino)-3-methylbutanoic acid were detected in the early stage, and some small molecular carboxylic acids such as fumaric, maleic, oxalic, and formic acids were identified in the later stage. The possible decomposition mechanism was proposed accordingly. Since the lead dioxide anode has been widely used for industrial production, 3DOM-PbO₂ would be a good alternative as a simple, efficient, and promising electrode material for wastewater remediation undoubtedly. It is believed that this facile strategy is scalable to prepare other macropore size-adjustable dimensionally stable anodes or various metal oxide films in the environment, energy conversion or storage fields.

Acknowledgments

This work was supported by National Natural Science Foundation of China (21077077 and 21277099).

Appendix A. Supplementary data

Supplementary data associated with this article can be found, in the online version, at <http://dx.doi.org/10.1016/j.apcatb.2013.08.046>.

References

- [1] E. Brillas, I. Sires, M.A. Oturan, Chemical Reviews 109 (2009) 6570–6631.
- [2] M. Panizza, G. Cerisola, Environmental Science and Technology 38 (2004) 5470–5475.
- [3] H. Liu, C. Wang, X.Z. Li, X.L. Xuan, C.C. Jiang, H.N. Cui, Environmental Science and Technology 41 (2007) 2937–2942.
- [4] M. Panizza, G. Cerisola, Chemical Reviews 109 (2009) 6541–6569.
- [5] C.A. Martinez-Huitle, A. De Battisti, S. Ferro, S. Reyna, M. Cerro-Lopez, M.A. Quiro, Environmental Science and Technology 42 (2008) 6929–6935.
- [6] C.A. Martinez-Huitle, E. Brillas, Applied Catalysis B: Environmental 87 (2009) 105–145.
- [7] S.Y. Yang, Y.S. Choo, S. Kim, S.K. Lim, J. Lee, H. Park, Applied Catalysis B: Environmental 111 (2012) 317–325.
- [8] P.R. Gogate, A.B. Pandit, Advances in Environmental Research 8 (2004) 501–551.
- [9] N. Oturan, J. Wu, H. Zhang, V.K. Sharma, M.A. Oturan, Applied Catalysis B: Environmental 140–141 (2013) 92–97.
- [10] H. Wang, Z.Y. Bian, G. Lu, L. Pang, Z.P. Zeng, D.Z. Sun, Applied Catalysis B: Environmental 125 (2012) 449–456.
- [11] X.P. Zhu, M.P. Tong, S.Y. Shi, H.Z. Zhao, J.R. Ni, Environmental Science and Technology 42 (2008) 4914–4920.
- [12] X.M. Chen, G.H. Chen, F.R. Gao, P.L. Yue, Environmental Science and Technology 37 (2003) 5021–5026.
- [13] Y.J. Feng, X.Y. Li, Water Research 37 (2003) 2399–2407.
- [14] N.J. Yang, H. Uetsuka, C.E. Nebel, Advanced Functional Materials 19 (2009) 887–893.
- [15] A.M.S. Solano, C.K.C. de Araujo, J.V. de Melo, J.M. Peralta-Hernandez, D.R. da Silva, C.A. Martinez-Huitle, Applied Catalysis B: Environmental 130 (2013) 112–120.
- [16] H.Y. Zhao, J.X. Gao, G.H. Zhao, J.Q. Fan, Y.B. Wang, Y.J. Wang, Applied Catalysis B: Environmental 136 (2013) 278–286.
- [17] J.P. Carr, N.A. Hampson, Chemical Reviews 72 (1972) 679–703.
- [18] R. Cossu, A.M. Polcaro, M.C. Lavagnolo, M. Mascia, S. Palmas, F. Renoldi, Environmental Science and Technology 32 (1998) 3570–3573.
- [19] M.H. Zhou, Q.Z. Dai, L.C. Lei, C. Ma, D.H. Wang, Environmental Science and Technology 39 (2005) 363–370.
- [20] S.-P. Tong, C.-A. Ma, H. Feng, Electrochimica Acta 53 (2008) 3002–3006.
- [21] G.H. Zhao, Y.G. Zhang, Y.Z. Lei, B.Y. Lv, J.X. Gao, Y.A. Zhang, D.M. Li, Environmental Science and Technology 44 (2010) 1754–1759.
- [22] C. Cominellis, Electrochimica Acta 39 (1994) 1857–1862.
- [23] B. Marselli, J. Garcia-Gomez, P.A. Michaud, M.A. Rodrigo, C. Cominellis, Journal of the Electrochemical Society 150 (2003) D79–D83.
- [24] J.D. Rodgers, W. Jedral, N.I. Bunce, Environmental Science and Technology 33 (1999) 1453–1457.
- [25] E. Guinea, F. Centellas, E. Brillas, P. Canizares, C. Saez, M.A. Rodrigo, Applied Catalysis B: Environmental 89 (2009) 645–650.
- [26] M.A. Oturan, M.C. Edelahi, N. Oturan, K. El Kacemi, J.J. Aaron, Applied Catalysis B: Environmental 97 (2010) 82–89.
- [27] R. Salazar, E. Brillas, I. Sires, Applied Catalysis B: Environmental 115 (2012) 107–116.
- [28] R. Amadelli, L. Armelao, A.B. Velichenko, N.V. Nikolenko, D.V. Girens, S.V. Kovalyov, F.I. Danilov, Electrochimica Acta 45 (1999) 713–720.
- [29] L.S. Andrade, L.A.M. Ruotolo, R.C. Rocha-Filho, N. Bocchi, S.R. Biaggio, J. Iniesta, V. Garcia-Garcia, V. Montiel, Chemosphere 66 (2007) 2035–2043.
- [30] Y. Liu, H.L. Liu, J. Ma, X. Wang, Applied Catalysis B: Environmental 91 (2009) 284–299.
- [31] M. Musiani, F. Furlanetto, P. Guerriero, Journal of Electroanalytical Chemistry 440 (1997) 131–138.
- [32] Y.W. Yao, C.M. Zhao, J. Zhu, Electrochimica Acta 69 (2012) 146–151.
- [33] X.H. Li, D. Pletcher, F.C. Walsh, Chemical Society Reviews 40 (2011) 3879–3894.
- [34] M.E. Hyde, R.M.J. Jacobs, R.G. Compton, Journal of Physical Chemistry B 108 (2004) 6381–6390.
- [35] B. Zhao, M.M. Collinson, Chemistry of Materials 22 (2010) 4312–4319.
- [36] A. Stein, Nature 468 (2010) 387–388.
- [37] J.X. Wang, Y.Z. Zhang, S.T. Wang, Y.L. Song, L. Jiang, Accounts of Chemical Research 44 (2011) 405–415.
- [38] D.C. Wu, F. Xu, B. Sun, R.W. Fu, H.K. He, K. Matyjaszewski, Chemical Reviews 112 (2012) 3959–4015.
- [39] S.J. Tian, J.J. Wang, U. Jonas, W. Knoll, Chemistry of Materials 17 (2005) 5726–5730.
- [40] C. Lopez, Advanced Materials 15 (2003) 1679–1704.
- [41] P.N. Bartlett, T. Dunford, M.A. Ghamem, Journal of Materials Chemistry 12 (2002) 3130–3135.
- [42] F.Q. Sun, W.P. Cai, Y. Li, B.Q. Cao, F. Lu, G.T. Duan, L.D. Zhang, Advanced Materials 16 (2004) 1116–1121.
- [43] A. Stein, F. Li, N.R. Denny, Chemistry of Materials 20 (2008) 649–666.
- [44] A. Topalov, D. Molnar-Gabor, J. Csanyi, Water Research 33 (1999) 1371–1376.
- [45] S. Song, J.Q. Fan, Z.Q. He, L.Y. Zhan, Z.W. Liu, J.M. Chen, X.H. Xu, Electrochimica Acta 55 (2010) 3606–3613.
- [46] G.H. Zhao, X. Cui, M.C. Liu, P.Q. Li, Y.G. Zhang, T.C. Cao, H.X. Li, Y.Z. Lei, L. Liu, D.M. Li, Environmental Science and Technology 43 (2009) 1480–1486.
- [47] Y. Lu, H.T. Yu, S. Chen, X. Quan, H.M. Zhao, Environmental Science and Technology 46 (2012) 1724–1730.
- [48] J. Wang, H.S. Yin, X.M. Meng, J.Y. Zhu, S.Y. Ai, Journal of Electroanalytical Chemistry 662 (2011) 317–321.
- [49] E.B. Cavalanti, S. Garcia-Segura, F. Centellas, E. Brillas, Water Research 47 (2013) 1803–1815.
- [50] E. Brillas, J. Casado, Chemosphere 47 (2002) 241–248.
- [51] C. Tai, J.F. Peng, J.F. Liu, G.B. Jiang, H. Zou, Analytica Chimica Acta 527 (2004) 73–80.
- [52] H.S. Kong, H.Y. Lu, W.L. Zhang, H.B. Lin, W.M. Huang, Journal of Materials Science 47 (2012) 6709–6715.
- [53] S. Abaci, K. Pekmez, T. Hokelek, A. Yildiz, Journal of Power Sources 88 (2000) 232–236.
- [54] J.L. Cao, H.Y. Zhao, F.H. Cao, J.Q. Zhang, Electrochimica Acta 52 (2007) 7870–7876.
- [55] Y.F. He, J.T. Feng, Y.Y. Du, D.Q. Li, ACS Catalysis 2 (2012) 1703–1710.
- [56] R. Amadelli, L. Armelao, E. Tondello, S. Daolio, M. Fabrizio, C. Pagura, A. Velichenko, Applied Surface Science 142 (1999) 200–203.
- [57] Y.Q. Cong, Z.C. Wu, Journal of Physical Chemistry C 111 (2007) 3442–3446.
- [58] D. Pavlov, B. Monahov, Journal of the Electrochemical Society 143 (1996) 3616–3629.
- [59] W. Kwon, J.-M. Kim, S.-W. Rhee, Electrochimica Acta 68 (2012) 110–113.
- [60] A. Dirany, I. Sires, N. Oturan, A. Ozcan, M.A. Oturan, Environmental Science and Technology 46 (2012) 4074–4082.
- [61] F.W. Wang, S.D. Li, M. Xu, Y.Y. Wang, W.Y. Fang, X.Y. Yan, Journal of the Electrochemical Society 160 (2013) D53–D59.
- [62] Y.A. Liu, H.L. Liu, J. Ma, J.J. Li, Electrochimica Acta 56 (2011) 1352–1360.
- [63] N.B. Tahar, A. Savall, Journal of the Electrochemical Society 145 (1998) 3427–3434.
- [64] H.S. Kong, W. Li, H.B. Lin, Z. Shi, H.Y. Lu, Y.Y. Dan, W.M. Huang, Surface and Interface Analysis 45 (2013) 715–721.
- [65] A.B. Velichenko, R. Amadelli, E.A. Baranova, D.V. Girens, F.I. Danilov, Journal of Electroanalytical Chemistry 527 (2002) 56–64.
- [66] C. Yuan, Y.D. Dai, C.H. Hung, Electrochimica Acta 86 (2012) 203–212.